Electronic Supplementary Material (ESI) for Journal of Materials Chemistry A.

Low-temperature-processed inorganic perovskite solar cells via solvent engineering with enhanced mass transport

Huachao Zai,[a,b] Deliang Zhang,[a] Liang Li,[c] Cheng Zhu,[a] Sai Ma,[a] Yizhou Zhao,[a] Zhiguo Zhao,[d] Changfeng Chen,[b] Huanping Zhou,[c] Yujing Li[a] and Qi Chen*[a]*

a. School of Materials Science and Engineering, Beijing Institute of Technology, Beijing 100081, P.R. China

b. Department of Materials Science and Engineering, College of Science, China University of Petroleum, Beijing 102249, P.R. China

c. Department of Materials Science and Engineering, College of Engineering, Peking University, Beijing 100871, P.R. China

d. Clean Energy Research Institute, China Huaneng Group, Beijing 102209, P.R. China

Experimental section

Materials. All reagents were used as received without further purification, including isopropanol (IPA, 99.99%, Sigma-Aldrich), SnO_2 (15% in H_2O colloidal dispersion liquid, Alfa Aesar), PbI_2 (99.999%, Sigma-Aldrich), $PbBr_2$ (99.999%, Sigma-Aldrich), CsI (99.999%, Sigma-Aldrich), N,N-dimethylformamide (DMF, 99.99%, Sigma-Aldrich), Dimethyl sulfoxide (DMSO, 99.9%, Sigma-Aldrich), chlorobenzene (CB, 99.9%, Sigma-Aldrich), PTAA (≥99.5%, Xi'an Polymer Light Technology Corp.), bis(trifluoromethane)sulfonimide lithium salt (Li-TFSI, 99.95%, Sigma-Aldrich), 4-tert-butylpyridine (tBP, 99.9%, Sigma-Aldrich), acetonitrile (ACN, 99.9%, Sigma-Aldrich) and ITO substrates.

Fabrication of solar cells. The indium tin oxide (ITO) coated glass was sequentially cleaned using detergent, ultra-pure water, and isopropanol. After 30 minutes of UV-O_3 treatments, the SnO_2 electron transport layers (ETLs) were spin-coated on ITO substrates from the SnO_2 colloidal solutions, and annealed on a hot plate at the displayed temperature of 150 °C for 30 min in ambient air. The $CsPbI_2Br$ precursor solution was prepared in a mixed solvent of DMF and DMSO with different volume ratios. The perovskite films were deposited onto the SnO_2 substrates with one-step spin coating procedures. The step was 3000 rpm for 30~150 s. The substrate was then immediately transferred on a hot plate and heated at 100 °C for 5 min. After cooling down to room temperature, the hole-transport layer was subsequently deposited on top of the perovskite film by spin coating at 3000 rpm for 30 s using a CB solution which contained PTAA, tBP and Li-TFSI. All operations were conducted in ambient atmosphere (temperature: 20 °C, relative humidity: 10%). Finally, 100 nm Au contact was deposited on top of Spiro-OMeTAD by thermal evaporation.

Characterizations. The thickness of films was measured with BRUKER DektakXT step profiler. Scanning electron microscope (SEM) images were measured using Hitachi S4800 field-emission scanning electron microscopy. X-ray diffraction (XRD) patterns were recorded by Rigaku D/Max 2,200 with Cu Kα as the X-ray source. The UV-visible absorption spectra were measured by Hitachi UH4150 spectrophotometer. PL spectra and TRPL spectra were obtained by FLS980 (Edinburgh Instruments Ltd) with an excitation at 510 nm. The J-V measurement was performed via the solar simulator (SS-F5-3A, Enlitech) along with AM 1.5G spectra whose intensity was calibrated by the certified standard silicon solar cell (SRC-2020, Enlitech) at 100mW/cm^2. Light intensity was calibrated with a National Institute of Metrology (China) calibrated KG5-filtered Si reference cell. The scanning speed of all J-V curves is 0.1 V/s. The effective area of cells were 0.1003 cm^2 and 1.0 cm^2 defined by masks for all the photovoltaic devices discussed in this work. The external quantum efficiency (EQE) data were obtained by using the solar-cell spectral-response measurement system (QE-R, Enlitech). A calibrated silicon diode with a known spectral response was used as a reference. The absorption and transmission spectra were measured by Hitachi UH4150 spectrophotometer.

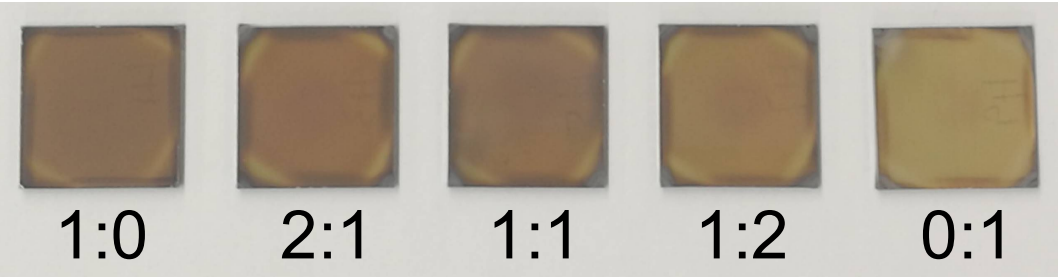

Figure S1. Optical image of perovskite films fabricated with different DMF: DMSO ratios (0.4 M).

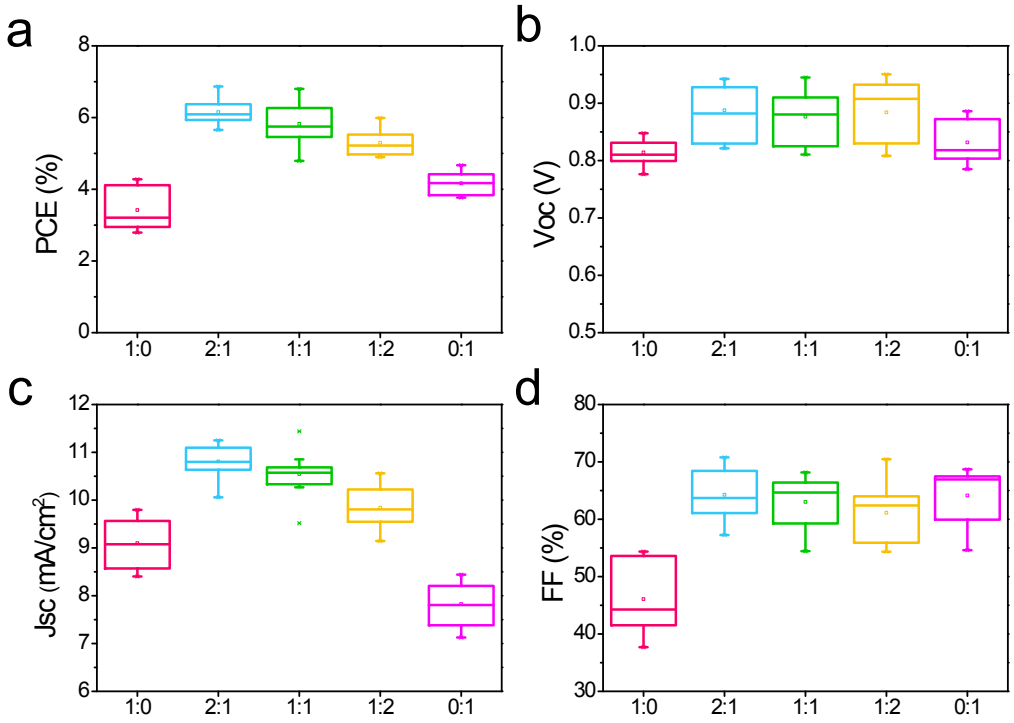

Figure S2. PV metrics for devices (~20 cells for each condition) fabricated with different DMF: DMSO ratios (0.4 M).

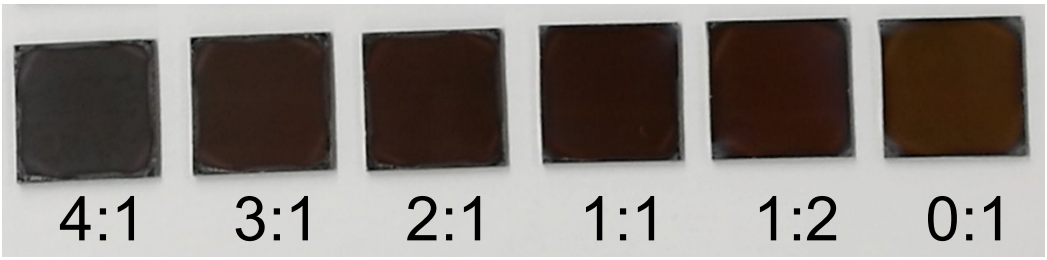

Figure S3. Optical image of perovskite films fabricated with different DMF: DMSO ratios (0.8 M).

Table S1. Thicknesses of the $CsPbI_2Br$ films fabricated with different DMF: DMSO ratios (0.8 M).

Samples	Thicknesses of the $CsPbI_2Br$ films (nm)					Average (nm)
4:1	303.63	303.86	308.10	304.80	306.70	305.418
3:1	302.76	296.08	309.85	308.20	307.20	304.818
2:1	303.17	296.38	306.03	289.61	308.40	300.718
1:1	266.99	297.28	291.61	303.69	285.74	289.062
1:2	231.81	285.27	276.68	278.12	287.57	271.890
0:1	224.84	209.10	223.42	223.18	213.42	218.792

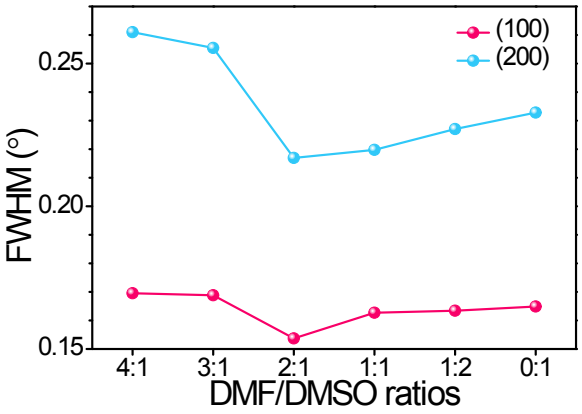

Figure S4. FWHM of (100) and (200) peaks for perovskite films fabricated with different DMF: DMSO ratios.

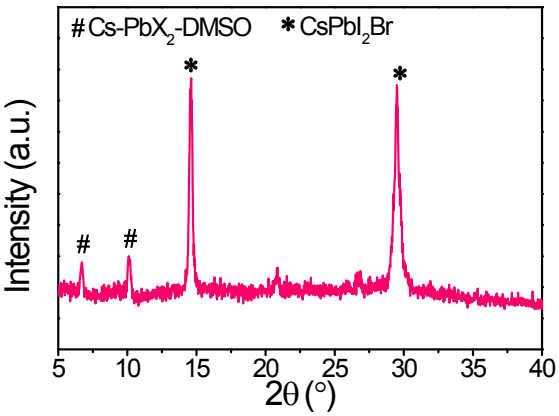

Figure S5. XRD pattern of the as spin-coated film fabricated with DMF/DMSO=2/1 before annealing.

Table S2. Carrier lifetimes for the $CsPbI_2Br$ films fabricated with different DMF: DMSO ratios.

Sample	τ_1 (ns)	τ_2 (ns)	A_1	A_2	τ_{ave} (ns)
4:1	4.58	10.51	0.93	0.07	4.98
3:1	5.15	11.37	0.90	0.10	5.74
2:1	6.63	12.10	0.86	0.14	7.40
1:1	5.85	11.45	0.87	0.13	6.58
1:2	3.20	6.37	0.81	0.19	3.82
0:1	2.38	4.79	0.52	0.48	3.53

Table S3. Urbach energies for the $CsPbI_2Br$ films fabricated with different DMF: DMSO ratios.

Sample	4:1	3:1	2:1	1:1	1:2	0:1
E_u (meV)	148.87	92.96	80.89	85.52	154.08	157.47

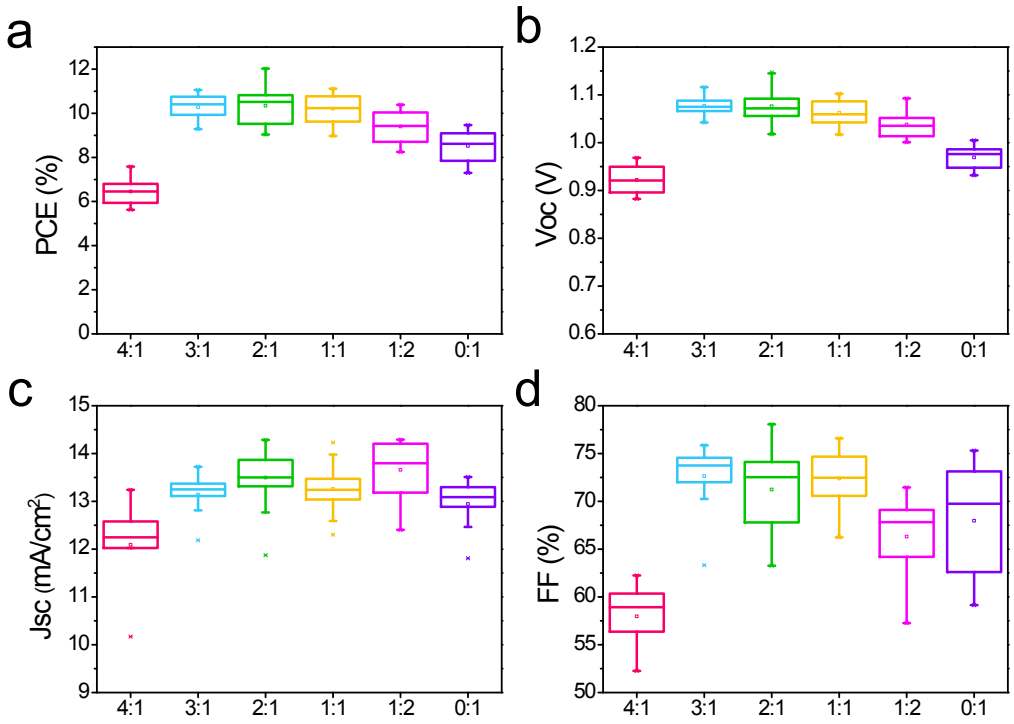

Figure S6. PV metrics for devices (~20 cells for each condition) fabricated with different DMF: DMSO ratios (0.8 M).

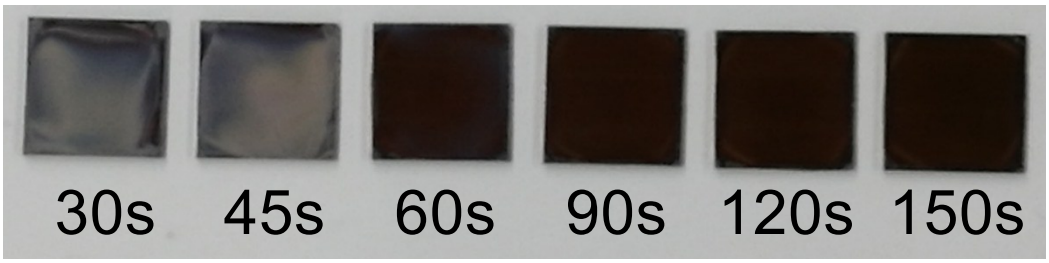

Figure S7. Optical image of perovskite films fabricated with different spin-coating time.

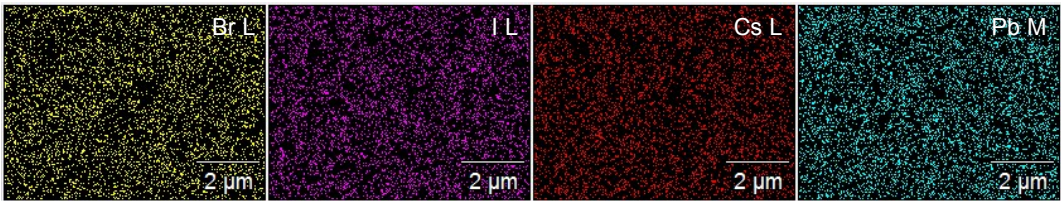

Figure S8. EDX mapping images for a perovskite film fabricated with 120 s.

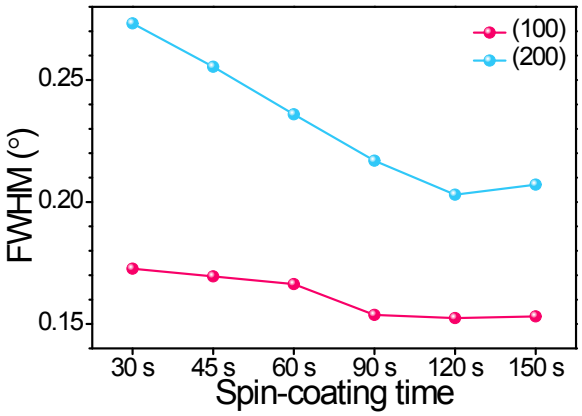

Figure S9. FWHM of (100) and (200) peaks for perovskite films fabricated with different spin-coating time.

Table S4. Thicknesses of the $CsPbI_2Br$ films fabricated with different spin-coating time.

Samples	Thicknesses of the $CsPbI_2Br$ films (nm)					Average (nm)
30 s	289.76	301.53	308.47	309.46	291.53	300.150
45 s	296.80	297.53	309.82	291.57	308.58	300.860
60 s	301.52	300.56	307.53	290.26	306.26	301.226
90 s	303.17	296.38	306.03	289.61	308.40	300.718
120 s	304.56	297.52	304.53	293.47	308.40	301.696
150 s	297.19	303.55	297.68	305.43	304.30	301.630

Table S5. Carrier lifetimes for the $CsPbI_2Br$ films fabricated with different spin-coating time.

Sample	τ_1 (ns)	τ_2 (ns)	A_1	A_2	τ_{ave} (ns)
30 s	2.47	13.38	0.99	0.01	2.61
45 s	2.83	5.71	0.89	0.11	3.15
60 s	3.92	6.81	0.67	0.33	4.86
90 s	6.63	12.10	0.86	0.14	7.40
120 s	6.79	14.17	0.65	0.35	9.41

150 s	6.84	12.83	0.68	0.32	8.76

Table S6. Urbach energies for the $CsPbI_2Br$ films fabricated with different spin-coating time.

Sample	30 s	45 s	60 s	90 s	120 s	150 s
E_u (meV)	161.99	160.34	112.28	80.89	61.55	73.28

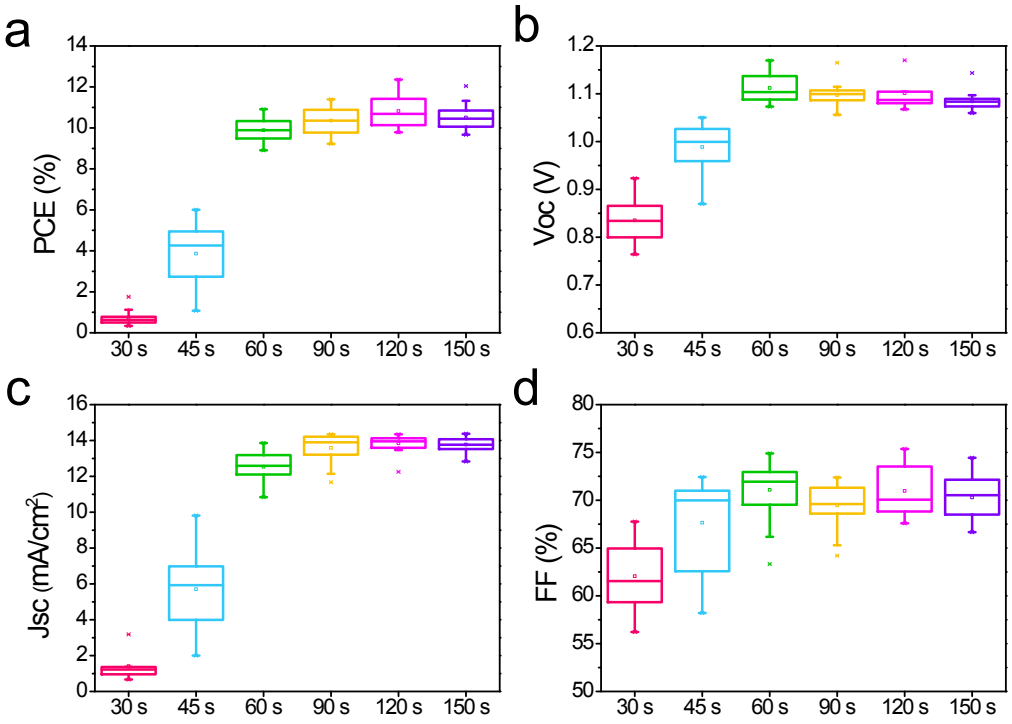

Figure S10. PV metrics for devices (~20 cells for each condition) fabricated with different different spin-coating time.

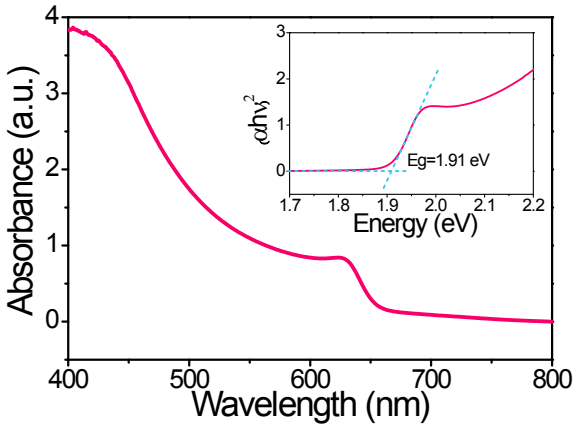

Figure S11. UV-vis absorption spectrum of the perovskite film fabricated with optimal condition, with an inset showing the Tauc plot.

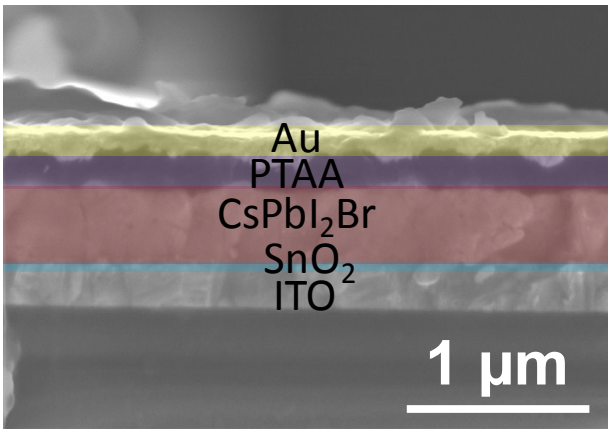

Figure S12. Cross-sectional SEM image of the optimal device.

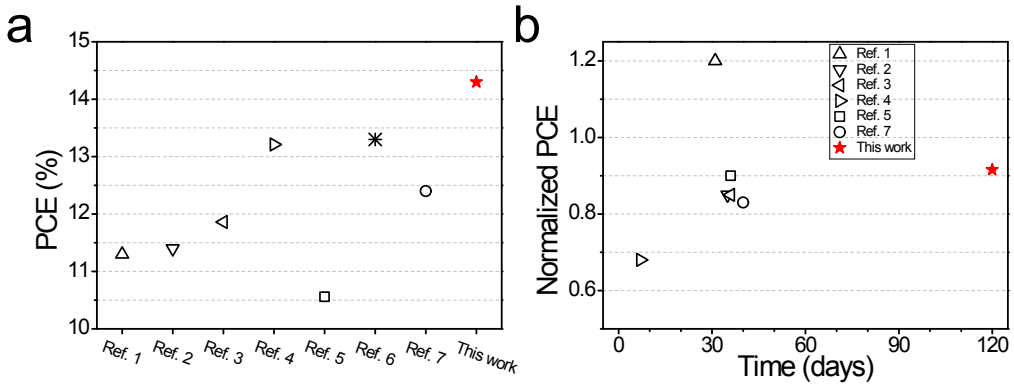

Figure S13. Comparison of (a) PCE and (b) long-term stability for inorganic perovskite solar cells with PCE over 10% via low-temperature process.[1-7]

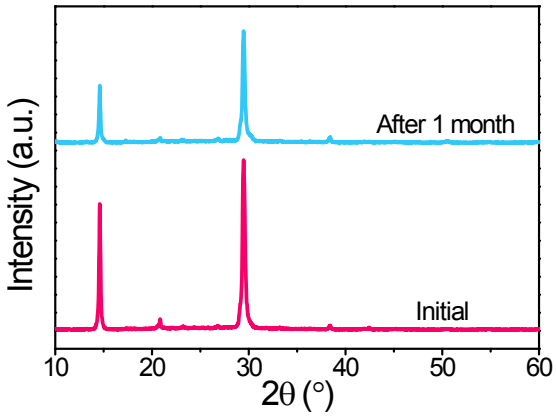

Figure S14. XRD patterns evolution of the $CsPbI_2Br$ film heated on a 100 °C hotplate in a nitrogen filled glove box.

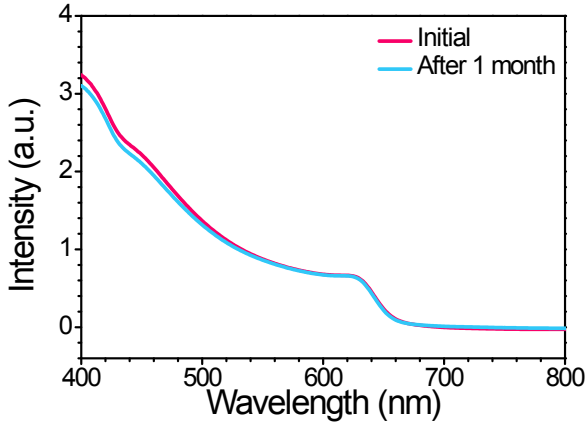

Figure S15. UV-vis spectra evolution of the $CsPbI_2Br$ film heated on a 100 °C hotplate in in a nitrogen filled glove box.

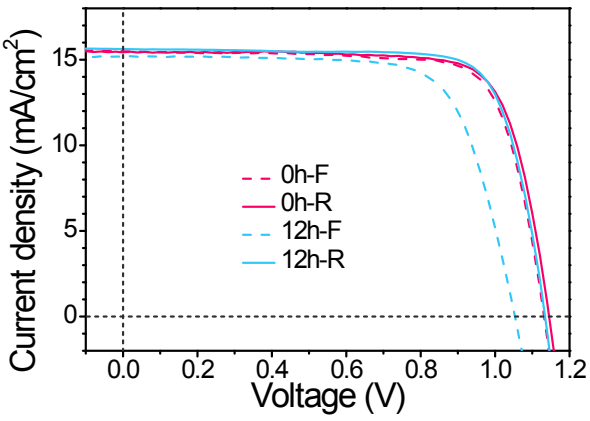

Figure S16. J-V curves for a device measured by forward and reverse scans with a 0.1 cm^2 active area before and after 12 h under continuous light soaking.

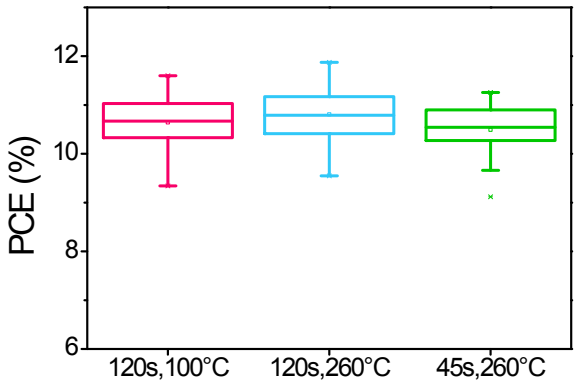

Figure S17. PCE for devices (~20 cells for each condition) fabricated with different spin-coating time and annealing temperature. (0.8 M)

References:

1. C. F. J. Lau, M. Zhang, X. Deng, J. Zheng, J. Bing, Q. Ma, J. Kim, L. Hu, M. A. Green, S. Huang and A. Ho-Baillie, *ACS Energy Lett.*, 2017, **2**, 2319-2325.

2. Q. Wang, X. Zheng, Y. Deng, J. Zhao, Z. Chen and J. Huang, *Joule*, 2017, **1**, 371-382.

3. T. Zhang, M. I. Dar, G. Li, F. Xu, N. Guo, M. Grätzel and Y. Zhao, *Science Advances*, 2017, **3**, e1700841.

4. Y. Hu, F. Bai, X. Liu, Q. Ji, X. Miao, T. Qiu and S. Zhang, *ACS Energy Lett.*, 2017, **2**, 2219-2227.

5. Y. Wang, T. Zhang, F. Xu, Y. Li and Y. Zhao, *Solar RRL*, 2018, **2**, 1700180.

6. C. Liu, W. Li, C. Zhang, Y. Ma, J. Fan and Y. Mai, *J. Am. Chem. Soc.*, 2018, **140**, 3825-3828.

7. Y. Jiang, J. Yuan, Y. Ni, J. Yang, Y. Wang, T. Jiu, M. Yuan and J. Chen, *Joule*, 2018, **2**, 1356-1368.